

## Drift kinetic effects on the resistive wall mode stability—Comparison between reversed field pinches and tokamaks

Z. R. Wang, S. C. Guo, and Y. Q. Liu

Citation: [Phys. Plasmas](#) **19**, 072518 (2012); doi: 10.1063/1.4737200

View online: <http://dx.doi.org/10.1063/1.4737200>

View Table of Contents: <http://pop.aip.org/resource/1/PHPAEN/v19/i7>

Published by the [American Institute of Physics](#).

---

### Related Articles

Oscillating plasma bubbles. III. Internal electron sources and sinks

[Phys. Plasmas](#) **19**, 082107 (2012)

Oscillating plasma bubbles. II. Pulsed experiments

[Phys. Plasmas](#) **19**, 082106 (2012)

On the existence of Weibel instability in a magnetized plasma. II. Perpendicular wave propagation: The ordinary mode

[Phys. Plasmas](#) **19**, 072116 (2012)

Long wavelength gradient drift instability in Hall plasma devices. I. Fluid theory

[Phys. Plasmas](#) **19**, 072112 (2012)

Cylindrical effects on Richtmyer-Meshkov instability for arbitrary Atwood numbers in weakly nonlinear regime

[Phys. Plasmas](#) **19**, 072108 (2012)

---

### Additional information on Phys. Plasmas

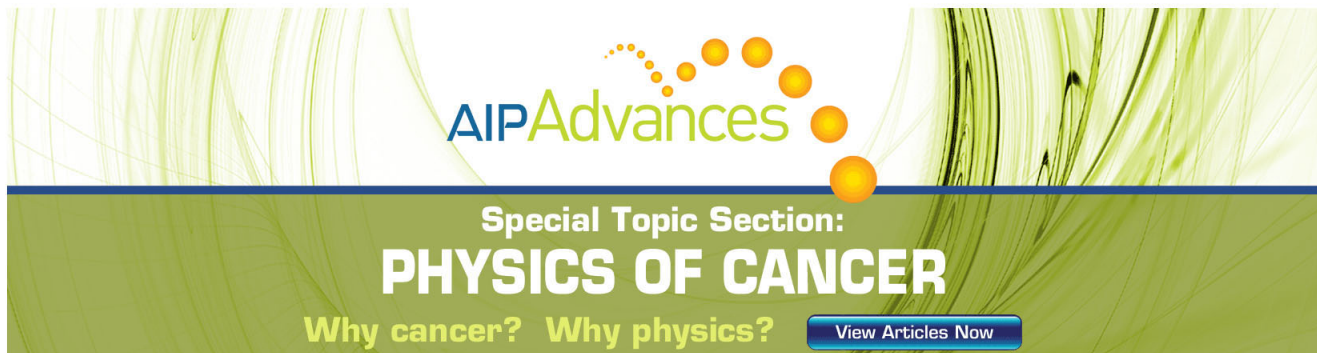
Journal Homepage: <http://pop.aip.org/>

Journal Information: [http://pop.aip.org/about/about\\_the\\_journal](http://pop.aip.org/about/about_the_journal)

Top downloads: [http://pop.aip.org/features/most\\_downloaded](http://pop.aip.org/features/most_downloaded)

Information for Authors: <http://pop.aip.org/authors>

## ADVERTISEMENT



**AIPAdvances**

Special Topic Section:  
**PHYSICS OF CANCER**

Why cancer? Why physics? [View Articles Now](#)

# Drift kinetic effects on the resistive wall mode stability—Comparison between reversed field pinches and tokamaks

Z. R. Wang,<sup>1</sup> S. C. Guo,<sup>1</sup> and Y. Q. Liu<sup>2</sup>

<sup>1</sup>*Consorzio RFX, Associazione Euratom ENEA sulla fusione, Corso Stati Uniti 4, Padova 35127, Italy*

<sup>2</sup>*Euratom/CCFE Fusion Association, Culham Science Centre, Abingdon, Oxon OX14 3DB, United Kingdom*

(Received 2 March 2012; accepted 4 June 2012; published online 26 July 2012)

The physics of kinetic effects on the resistive wall mode (RWM) stability is studied, and a comparison between reversed field pinch (RFP) and Tokamak configurations is made. The toroidal, magnetohydrodynamic (MHD)-kinetic hybrid stability code MARS-K, in which the drift kinetic effects are self-consistently incorporated into the MHD formulation, is upgraded with an extensive energy analysis module. In the tokamak configuration, the kinetic effect can stabilize the mode with very slow, or vanishing plasma rotation, due to the mode resonance with the toroidal precession drift of thermal trapped particles. In RFP, instead, stabilization of the RWM comes mainly from the ion acoustic Landau damping (i.e., the transit resonance of passing particles). In the high beta region, the critical flow rotation frequency required for the mode stabilization is predicted to be in the ion acoustic range. Detailed physical analyses, based on the perturbed potential energy components, have been performed to gain understanding of the stabilizing mechanism in the two different systems. [<http://dx.doi.org/10.1063/1.4737200>]

## I. INTRODUCTION

Understanding physics and stabilization of the resistive wall mode (RWM) is an important task for the successful operation of the present day and future fusion devices. The RWM is generally a global kink-like, non-axisymmetric instability, with the growth rates significantly reduced by the surrounding conducting wall(s). For advanced tokamak scenarios, including those foreseen for ITER,<sup>1</sup> and aiming at simultaneous maximization of the plasma pressure and a steady state operation, the RWM poses a severe pressure limit.<sup>2,3</sup> For reversed field pinch (RFP) plasmas, the RWM appears as potentially disruptive instability, whenever the duration of the discharge is longer than the penetration time of the passive conducting structure (resistive wall).

Two general methods are known for the RWM stabilization: the active control and the so-called “passive control.” For the active control, the perturbed magnetic field (or voltage) is measured by a set of sensor loops outside the plasma, and is used to generate the control signal for a set of active magnetic coils. Such mechanism has been extensively studied theoretically<sup>4–11,45</sup> and has been successfully applied in the present day fusion experiments.<sup>12–17,46</sup> The “passive control,” also often referred to as “rotational stabilization,” relies on a mechanism, where the RWM suppression is achieved via plasma flow combined with various dissipations such as the presence of plasma viscosity, resistivity, the continuum spectra damping (the Alfvén continuum and/or the ion acoustic damping), as well as kinetic resonances with particle drift motions. A large number of studies, by both theory and experiments, have shown that in tokamak plasmas, the RWM can be suppressed by a plasma rotation.<sup>18–21</sup> In particular, recent experimental development on the RWM study has indicated that a very slow, sometimes maybe even vanishing plasma rotation, can stabilize the mode in tokamak

plasmas.<sup>22–24</sup> Theoretical model has been proposed for the explanation, where the main dissipation channel of the free energy is the mode resonance with the precession drift motion of trapped particles.<sup>25–27</sup> In RFPs, instead, the presently operating devices have not given indication of the rotational stabilization. Theoretical studies in fluid theory, taking into account the plasma viscosity and continuum damping, predicted that the plasma flow velocity, required for the RWM stabilization, was in the Alfvén velocity range.<sup>28,29</sup> Such a high velocity is not achieved in the present day RFP experiments. On the other hand, it is not clear whether a plasma regime can be found for RFP plasmas, where the RWM can be stabilized at a slower (than the Alfvén speed) plasma flow, and where the mode stabilization is provided by drift kinetic damping. Recent study<sup>30</sup> did not find such a plasma regime in RFP. This work shows that the RWM can be fully suppressed by kinetic effects, in a high  $\beta$  RFP plasma. In addition, an energy analysis of the mode stabilization physics is performed in this paper. The RFP configuration does not impede obtaining high  $\beta_p$  plasmas, which should be achievable in future RFP devices. In fact even in a presently operating RFP device (MST), the  $\beta_p$  value can be reached up to 20%,<sup>31</sup> by performing the so-called pulsed poloidal current drive (PPCD). Unfortunately, the presence of a thick wall in MST prevents a direct experimental study of the RWM instability.

In this work, we investigate the kinetic resonant effects on the RWM stability for both RFPs and tokamaks. We perform detailed comparison of the physical mechanisms for the mode damping in the two configurations. Since RFP normally possesses a circular cross section for the plasma shape, we also consider tokamak plasmas with a circular shape, in order to exclude additional shaping effects. The non-perturbative MHD-kinetic hybrid toroidal stability code MARS-K (Ref. 32) is used for this study. In this approach, the drift kinetic theory cooperates with the MHD equation

via the perturbed kinetic pressure tensor. Therefore, it allows the kinetic effect, as the same order as MHD part, to modify the complex eigenfunction and the eigenvalue. A new module for computing various potential energy components has been integrated into the code, allowing in-depth analyses and a better understanding of the physical mechanisms behind computational results. A detailed comparative study of the kinetic-modified RWM stability between the two systems, tokamaks and RFPs, provides very useful insights into the physics of the passive stabilization of the modes.

## II. MODEL AND FORMULATIONS

### A. Toroidal self-consistent kinetic model

The MARS-K code numerically solves the linearized, single-fluid MHD equations with self-consistent inclusion of drift kinetic resonances in toroidal geometry.<sup>32</sup> For a given curvilinear flux coordinate system  $(s, \chi, \phi)$ , and by assuming that all the perturbations have the form  $A(s, \chi, \phi, t) = A(s, \chi)e^{-i\omega t - in\phi}$ , we can write the core equations, involving the kinetic terms, in the Eulerian frame:

$$-i(\omega + n\Omega)\xi = \mathbf{v} + (\xi \cdot \nabla\Omega)R^2\nabla\phi \quad (1)$$

$$\begin{aligned} -i\rho(\omega + n\Omega)\mathbf{v} &= -\nabla \cdot \mathbf{p} + \mathbf{j} \times \mathbf{B} + \mathbf{J} \times \mathbf{Q} \\ &\quad - \rho[2\Omega\hat{\mathbf{Z}} \times \mathbf{v} + (\mathbf{v} \cdot \nabla\Omega)R^2\nabla\phi] \end{aligned} \quad (2)$$

$$-i(\omega + n\Omega)\mathbf{Q} = \nabla \times (\mathbf{v} \times \mathbf{B}) + (\mathbf{Q} \cdot \nabla\Omega)R^2\nabla\phi \quad (3)$$

$$i(\omega + n\Omega)p = \mathbf{v} \cdot \nabla P \quad (4)$$

$$\mathbf{j} = \nabla \times \mathbf{Q}, \quad (5)$$

where  $s$  is the normalized radial coordinate, labeling the equilibrium flux surface,  $\chi$  is a generalized poloidal angle.  $\omega = i\gamma - \omega_r$  is the complex eigenvalue of the mode ( $\gamma$  being the mode growth rate,  $\omega_r$  the mode rotation frequency in the laboratory frame). The mode frequency is corrected by a Doppler shift  $in\Omega$ , with  $n$  being the toroidal mode number,  $\Omega$  the plasma rotation frequency in the toroidal direction  $\phi$ .  $\xi$ ,  $\mathbf{v}$ ,  $\mathbf{Q}$ ,  $\mathbf{j}$ ,  $\mathbf{p}$  represent the perturbed quantities: the plasma displacement, the perturbed velocity, magnetic field, current, and pressure tensor, respectively.  $\rho$  is the unperturbed plasma density.  $R$  is the plasma major radius.  $\hat{\mathbf{Z}}$  is the unit vector in the vertical direction.  $\mathbf{B}$ ,  $\mathbf{J}$ , and  $P$  denote the equilibrium magnetic field, current, and pressure, respectively. A conventional unit system is assumed with the vacuum permeability  $\mu_0 = 1$ . For the RWM study, a set of vacuum equations for the magnetic field  $\mathbf{Q}$ , and the resistive wall equation based on the thin-shell approximation, are solved together with Eqs. (1)–(5).<sup>8</sup> The plasma resistive term in the Ohm's law is dropped. Note that the ordinary  $5/3 P \nabla \cdot \mathbf{v}$  term is dropped from Eq. (4) for the perturbed fluid pressure. This term is replaced by the drift kinetic terms which enter into the MHD equations via the perturbed kinetic pressure tensor

$$\mathbf{p} = p\mathbf{I} + p_{\parallel}\hat{\mathbf{b}}\hat{\mathbf{b}} + p_{\perp}(\mathbf{I} - \hat{\mathbf{b}}\hat{\mathbf{b}}), \quad (6)$$

which in turn is self-consistently included into the MHD formulation via the momentum Eq. (2). In Eq. (6),  $\hat{\mathbf{b}} = \mathbf{B}/B$ ,

$B = |\mathbf{B}|$ ,  $\mathbf{I}$  is the unit tensor.  $p$  is the scalar fluid pressure perturbation,  $p_{\parallel}(\xi_{\parallel})$ ,  $p_{\perp}(\xi_{\perp})$  are the parallel and perpendicular perturbations of the kinetic pressure, respectively, and are computed via

$$p_{\parallel}e^{-i\omega t - in\phi} = \sum_{e,i} \int d\Gamma M v_{\parallel}^2 f_L^1 \quad (7)$$

$$p_{\perp}e^{-i\omega t - in\phi} = \sum_{e,i} \int d\Gamma \frac{1}{2} M v_{\perp}^2 f_L^1. \quad (8)$$

The summation in Eqs. (7) and (8) is over the electron and ion components. The integral is carried out over the particle velocity space  $\Gamma$ .  $M$  is the particle mass,  $v_{\parallel}$ ,  $v_{\perp}$  are the parallel and perpendicular velocity components of the particle.  $f_L^1$  is the perturbed particle distribution function, which is derived by solving the perturbed drift kinetic equation for each particle species, following approaches by Antonsen<sup>33</sup> and Porcelli.<sup>34</sup> The expression for  $f_L^1$  is

$$f_L^1 = -f_e^0 \varepsilon_k e^{-i\omega t - in\phi} \sum_{m,l} X_m H_{ml} \lambda_{ml} e^{in\tilde{\phi}(t) + im\langle \dot{\chi} \rangle t + il\omega_b t}, \quad (9)$$

where  $f_e^0$  is the energy derivative of the particle equilibrium distribution function (which is assumed Maxwellian for thermal particles).  $\varepsilon$  is the particle's total energy.  $\varepsilon_k = \varepsilon - Ze\Phi$  is the kinetic energy of the particle, with  $\Phi$  being the equilibrium electrostatic potential and  $Ze$  the particle charge.  $\tilde{\phi}(t) = \phi(t) - \langle \dot{\phi} \rangle t$  denotes the periodic part of the particle motion projected along the toroidal direction with  $\langle \cdot \rangle$  meaning the average over the particle bounce period.  $m$  and  $n$  correspond to the harmonic numbers in toroidal and poloidal directions, respectively.  $l$  is the harmonic number in the bounce orbit expansion.  $X_m$  and  $H_{ml}$  both relate to the perturbed particle Lagrangian,<sup>32</sup> with  $X_m$  denoting the poloidal Fourier harmonics of the perpendicular fluid displacement and the magnetic field perturbation;  $H_{ml}$  denoting the geometrical factor associated with the equilibrium quantities.  $\lambda_{ml}$  represents the mode-particle resonance condition,

$$\lambda_{ml}^{\alpha} = \frac{n[\omega_{*N} + (\hat{\varepsilon}_k - 3/2)\omega_{*T} + \Omega] + \omega}{n\omega_d - [\alpha(m - nq) + l]\omega_b + n\Omega + \omega + i\nu_{eff}}, \quad (10)$$

where  $\omega_{*N}$  and  $\omega_{*T}$  are the diamagnetic drift frequencies due to the plasma density and temperature gradients, respectively. In the above solution of the drift kinetic equation, it has been assumed that the effect of finite radial excursion width of particles across magnetic surfaces is negligible.  $q$  is the safety factor,  $\nu_{eff}$  is the effective collision frequency,  $\hat{\varepsilon}_k = \varepsilon_k/T$  is the particle kinetic energy normalized by the temperature.  $\omega_d$  is the bounce-orbit-averaged precession drift frequency. For trapped particles,  $\alpha = 0$ , and  $\omega_b$  is the bounce frequency. For passing particles,  $\alpha = \sigma$ ,  $\sigma = \text{sign}(v_{\parallel})$ , and  $\omega_b$  represents the transit frequency. In further discussions we also use a notation  $\omega_p$  for the transit frequency, in order to be distinguished from the bounce frequency. Equation (10) includes particle bounce, transit, as well as magnetic

precession drift resonances with the mode. The imaginary part of the resonant operator represents the energy transfer between the mode and particles. A simple collisionality effect is also included into the resonant operator, with a detailed derivation reported in Ref. 32.

We note that the self-consistent approach allows kinetic modification of the RWM eigenfunction. Moreover, the unknown eigenvalue  $\omega$  enters into the resonance operator (10). This is an important aspect of the self-consistency of the kinetic formulation, which requires an iterative loop for numerically finding the converged eigenvalue.

## B. Quadratic energy terms

In order to gain better physical understanding, we compute various components of the quadratic energy form, for both fluid and drift kinetic energy perturbations, from the self-consistent solution. An energy analysis module have been developed and integrated into the MARS-K code.

As well known, the quadratic energy form can be constructed by multiplying Eq. (2) by  $\xi_{\perp}^*$  and integrating over the plasma volume  $V^P$ .<sup>35,36</sup> We then define the following energy components of the fluid potential energy  $\delta W_F$  and the kinetic potential energy  $\delta W_K$

$$\delta W_F = \delta W_{mb} + \delta W_{mc} + \delta W_{pre} + \delta W_{cur} \quad (11)$$

$$\delta W_{mb} = \frac{1}{2} \int_{V^P} |\mathbf{Q}_{\perp}|^2 J ds d\chi d\phi \quad (11a)$$

$$\delta W_{mc} = \frac{1}{2} \int_{V^P} B^2 |\nabla \cdot \xi_{\perp} + 2\xi_{\perp} \cdot \kappa|^2 J ds d\chi d\phi \quad (11b)$$

$$\delta W_{pre} = -\frac{1}{2} \int_{V^P} (\xi_{\perp} \cdot \nabla P) (\kappa \cdot \xi_{\perp}^*) J ds d\chi d\phi \quad (11c)$$

$$\delta W_{cur} = -\frac{1}{2} \int_{V^P} J_{\parallel} (\xi_{\perp}^* \times \mathbf{b}) \cdot \mathbf{Q}_{\perp} J ds d\chi d\phi, \quad (11d)$$

where  $J$  is the Jacobian of the flux coordinates,  $\kappa$  is the curvature of the magnetic field line.  $\delta W_{mb}$  is the magnetic bending term representing the energy required to bend magnetic field lines,  $\delta W_{mc}$  corresponds to the energy necessary to compress the magnetic field. Both terms are positive and give stabilizing contributions.  $\delta W_{pre}$  and  $\delta W_{cur}$  represent potential sources of instability, and are referred to as the pressure driven and the current driven terms, respectively. Both  $\delta W_{pre}$  and  $\delta W_{cur}$  can be negative. We consider cases with vanishing perturbed surface current, where the surface terms in the potential energy disappear. In the energy calculation, For the slow rotation we investigate in present work, we neglect the Coriolis force terms in the RHS of Eq. (2). The kinetic pressure tensor term in Eq. (2) leads to a volumetric drift kinetic energy

$$\delta W_K = \frac{1}{2} \int_{V^P} J ds d\chi d\phi \left[ p_{\perp} \frac{1}{B} (Q_{\parallel}^* + \nabla B \cdot \xi_{\perp}^*) + p_{\parallel} \kappa \cdot \xi_{\perp}^* \right] \quad (12)$$

as well as a surface term  $\frac{1}{2} \int_{S^P} \tilde{p}_{\perp} \xi_{\perp}^* \cdot \mathbf{n} J_s d\chi d\phi$ , which is negligible if the equilibrium pressure vanishes at the plasma edge  $P=0$  (the perturbed kinetic pressure is roughly proportional to the equilibrium pressure).  $S^P$  here is the plasma surface,  $J_s = |\nabla s| J$  the surface Jacobian,  $\mathbf{n}$  an outward normal vector to the vacuum region.

We also compute the vacuum energy  $\delta W_{v\infty}$  and  $\delta W_{vb}$ , without wall and with an ideal wall at the minor radius  $b$ , respectively

$$\delta W_{v\infty} = \frac{1}{2} \int_{V^{\infty}} |\mathbf{Q}|^2 J ds d\chi d\phi = -\frac{1}{2} \int_{S^P} b_1^n \hat{V}_1^{*\infty} J_s d\chi d\phi, \quad (13)$$

$$\delta W_{vb} = \frac{1}{2} \int_{V^b} |\mathbf{Q}|^2 J ds d\chi = -\frac{1}{2} \int_{S^P} b_1^n \hat{V}_1^{*b} J_s d\chi d\phi, \quad (14)$$

where  $b_1^n$  is the normal magnetic field perturbation;  $\hat{V}_1^{*\infty,b}$  the complex conjugate of the perturbed magnetic scalar potential, which is determined by the ideal wall position and  $b_1^n$  at the plasma surface.<sup>36</sup> The two energy terms (13) and (14) are associated with the vacuum magnetic field perturbation, induced by the plasma instability. They are always positive and play a stabilizing role for the RWM.  $\delta W_{v\infty}$  and  $\delta W_{vb}$  can be written either in a volume integral, or in a surface integral as shown in Eqs. (13) and (14).

Equations (11)–(14) are implemented in the MARS-K code, and applied for the energy analysis of the RWM physics in the present work.

## III. CHARACTERISTICS OF FLUID RWM IN RFPS AND TOKAMAKS

Although RWMs share certain similar behaviour in both tokamaks and RFPS, there are a few dissimilarities resulted from the differences between the two configurations that lead to different conditions for the mode stabilization. We find that the kinetic effects work differently on the RWM instability as well in the two devices. In this section, we will describe the differences between the two configurations, and the resulting dissimilarities of the RWM characteristics in the fluid approximation.

As well known, in tokamaks, RWMs are often driven by the plasma pressure. The RWM instability appears in the range of  $\beta_N$  values (normalized  $\beta$ ) between the so-called no-wall limit  $\beta_N^{\text{no-wall}}$  and the ideal wall limit  $\beta_N^{\text{ideal-wall}}$ .<sup>37</sup> In RFPS, RWMs are the current driven modes instead. The reason is that the RFP possesses a stronger poloidal magnetic field, reaching the same order of the field strength as the toroidal field. This implies a larger plasma current in RFPS than in tokamaks, for the same value of the toroidal field. Therefore, the plasma is easier to be “kinking” due to the weaker toroidal field. In fact, ideal external kink instability is easier to be driven by the large plasma current in RFP. Obviously, for the current driven RWMs, the no-wall beta limit is zero, i.e.,  $\beta_N^{\text{no-wall}} = 0$ .

Furthermore, due to the toroidal field reversion, resulted from the relaxation process, RFPS can operate in the stable regime of the “resonant” (with rational surface being inside the plasma) ideal kink modes. The RWM instabilities always have their rational surfaces outside the plasma. They can be



the so-called “externally non-resonant” modes (ENRM), if the rational surfaces are located at  $q < q(a) < 0$  ( $q(a)$  is the safety factor at the plasma edge  $r = a$ ), or the “internally non-resonant” modes (INRM), if the rational surfaces are located at  $q > q(0) > 0$ .<sup>11,38,39</sup> We choose  $n > 0$ , it means for a given  $n$  number, each poloidal harmonic with  $m > 0$  corresponds to INRM; the poloidal harmonics with  $m < 0$  represents ENRMs. In tokamaks instead, RWMs can have their rational surfaces inside the plasma, and/or outside the plasma. The difference in the location of rational surfaces (non-resonant versus resonant) results in different conditions for the mode stabilization. In RFP, the MHD theory, with classical viscous dissipation in cylindrical geometry, has predicted<sup>28,29</sup> that the required toroidal plasma rotation velocity  $V_{oc}$ , for full stabilization of the RWM, is in the range of the Alfvén velocity (around  $0.2V_{A\theta}$ – $1.0V_{A\theta}$ , where  $V_{A\theta}$  is Alfvén velocity defined by the equilibrium poloidal magnetic field). The value of  $V_{oc}$  varies with the mode number and the equilibrium parameters. In the case of a resistive wall located near the plasma edge, the critical velocity required for the stabilization satisfies the condition  $kV_{oc} \approx \min\{(k_{\parallel}V_A)_{r=a}, (k_{\parallel}V_A)_{r=0}\}$ ,<sup>29</sup> where  $k_{\parallel}$  and  $k$  are the parallel and toroidal mode wave numbers, respectively. Since both INRM and ENRM, being the non-resonant modes, have their rational surfaces far from the plasma edge,  $k_{\parallel}(a)$  and/or

$k_{\parallel}(0)$  are larger ( $k_{\parallel}(a) \sim 0.2$ – $1$  for the RFPs) than that of the RWM in tokamaks (where  $k_{\parallel}(a) \approx 0$  often holds). Therefore, the rotational stabilization of RWMs in RFPs requires higher  $V_{oc}$  than in tokamaks. In fact, in tokamaks, the MHD theory predicted  $V_{oc}$  is in the range of the ion sound speed (only a few percent of the Alfvén velocity).<sup>18–21</sup>

Finally, in RFPs the strong poloidal field makes the poloidal asymmetry weaker than that in tokamaks, leading to a less important role of the toroidal effects. From another point of view, it can be understood that the stronger poloidal field makes lower  $q$  ( $q$  is the safety factor) configurations; and the distance between the two neighboring rational surfaces, corresponding to two neighboring poloidal mode numbers (e.g.,  $m/n$  and  $(m \pm 1)/n$ ), is much larger than that in tokamaks. This causes weaker toroidal mode coupling in RFPs than in tokamaks. Furthermore, compared with tokamaks, the magnetic field curvature in RFPs is dominated by the poloidal field, so the “bad curvature” region extends to the whole poloidal angle, resulting in a weak ballooning structure for the mode.

Figure 1 compares the typical eigenfunctions (the radial displacement  $\xi_n$ ) of the RWM, computed by MARS-K, for the two different configurations. Figures 1(a) and 1(b) show the modes in RFP, with  $n = 6$  at  $\varepsilon = a/R = 0.2295$ , and  $n = 4$  at  $\varepsilon = 0.4$ , respectively. The parameters  $F$  and  $\Theta$  are defined

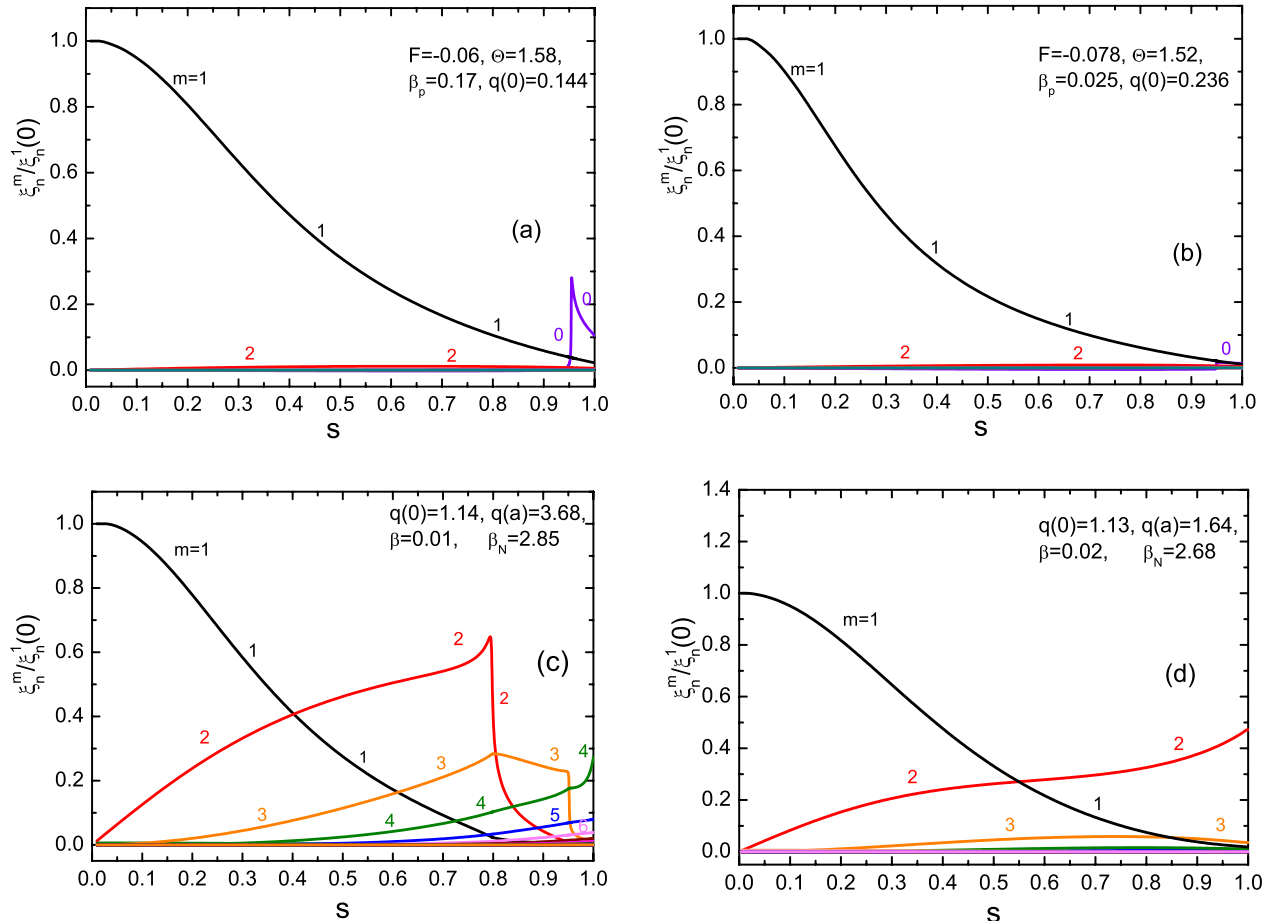


FIG. 1. The poloidal Fourier harmonics of the normal component of the plasma displacement, plotted along the minor radius, for the fluid RWM in (a) RFP with aspect ratio  $\varepsilon = a/R = 0.2295$  and  $n = 6$ , (b) RFP with  $\varepsilon = 0.4$  and  $n = 4$ , (c) tokamak with  $q(a) = 3.68$ ,  $q(0) = 1.14$ , and  $n = 1$  (d) tokamak with  $q(a) = 1.64$ ,  $q(0) = 1.13$ , and  $n = 1$ . A straight field line coordinate system is used. No plasma rotation is assumed.

as  $F = B_\phi(a)/\langle B_\phi \rangle$ , and  $\Theta = B_\chi(a)/\langle B_\phi \rangle$ , where  $B_\phi(a)$  and  $B_\chi(a)$  are the toroidal and poloidal magnetic fields in the plasma edge, respectively,  $\langle B_\phi \rangle$  is the volume average of the toroidal magnetic field. In the RFP plasma, for the unstable  $n=6$  mode, only the  $m=1$  poloidal harmonic has a large radial displacement. The other poloidal harmonics ( $m = -1, \pm 2, \pm 3, \pm 4, \dots$ ) appear with much smaller amplitude. This is the consequence of the weak toroidal coupling in the RFP configuration. Figure 1(b) plots the eigenfunction for a smaller aspect ratio (“fat”) RFP with  $\varepsilon = 0.4$ , again showing the weak toroidal coupling. Figures 1(a) and 1(b) indicate that the toroidal coupling effect in RFP is almost independent of the aspect ratio. We also note the peaking of the  $m=0$  harmonic, occurring at the  $m=0$  rational surface.

Figures 1(c) and 1(d) plot the radial displacements  $\xi_n$  of the RWM in the tokamak configuration with a circular cross-section. Figure 1(c) shows a case for the  $n=1$  pressure driven RWM, with  $q(0) = 1.14$ ,  $q(a) = 3.68$ , and  $\beta = 0.01$ . There are two rational surfaces  $q=2$  and  $q=3$  located inside the plasma for this case. Figure 1(d) shows a case for the  $n=1$  current driven mode, with  $q(0) = 1.13$ ,  $q(a) = 1.64$ , and  $\beta = 0.02$ . There is no rational surface inside the plasmas. Both figures show a strong toroidal coupling effect, where multiple poloidal harmonics co-exist with sufficiently large amplitudes, all contributing to the  $n=1$  mode growth rates. The sharp radial variation of the  $m=2$  and  $m=3$  harmonics, shown in Fig. 1(c), indicates the Alfvén resonance near the  $q=2$  and  $q=3$  rational surfaces, respectively.

Figure 2 compares the 2D mode structure, in the toroidal cross-section, between the RFP [Fig. 2(a)] and tokamak [Fig. 2(b)] plasmas. The two cases correspond to the eigenfunctions shown in Figs. 1(a) and 1(c), respectively. The RWM in the RFP, with the sole  $m=1$  dominant mode, has almost no ballooning character. On the contrary, the tokamak RWM has multiple poloidal harmonics growing together, and exhibiting obvious ballooning character. Only the real components of  $\xi_n$  are plotted in both figures.

#### IV. DRIFT KINETIC EFFECTS ON RWM IN RFPS AND TOKAMAKS

In this section, MARS-K code is applied for the RWM study in both RFP and tokamak configuration. The MHD-kinetic hybrid, self-consistent formulation, presented in Sec. II, is followed. The wave-particle interaction is included into the MHD equations via the pressure tensor term, and described by the resonant operator (10), for each particle species. The drift kinetic potential energy  $\delta W_k$ , presented in Sec. II, can be written as<sup>26</sup>

$$\delta W_K = \frac{\nu\sqrt{\pi}}{2B_0} \sum_{e,i} \int d\Psi P_{e,i} \left\{ \int d\hat{\varepsilon}_k \hat{\varepsilon}_k^{5/2} e^{-\hat{\varepsilon}_k} \sum_{\sigma} \times \left[ d\Lambda \sum_l \lambda_l^\alpha \hat{\tau}_b | \langle e^{-i(l+\alpha n q)\omega_{bt} - i n \phi} H_L \rangle_l |^2 \right] \right\}, \quad (15)$$

where  $\Psi$  is the equilibrium poloidal flux,  $P_{e,i}$  the ion and electron equilibrium pressure,  $\Lambda = B_0 \mu / \varepsilon_k$ , with  $B_0$  being the on-axis field strength).  $H_L$  is the particle perturbed Lagrangian.<sup>32</sup> The integration is carried out in both real and velocity spaces. The sum is over the poloidal Fourier  $m$  and bounce harmonics  $l$  the passing and trapped particles, as well as the particle species ( $e, i$ ). For trapped particles,  $\alpha = 0$ ,  $\nu = 1/2$ , and  $\hat{\tau}_b$  is the particle bounce period normalized by a factor  $\sqrt{M/2\varepsilon_k}$ ; for passing particles,  $\alpha = 1$ ,  $\nu = 1$ , and  $\hat{\tau}_b$  denotes the normalized transit period. In this study, we consider the mode resonance with the precession frequencies of trapped particles (both ions and electrons), the ion bounce frequency, and the transit frequency of passing ions. These are the most important effects in the current study. In the following, the words “full kinetic” refer to the combined resonant effects mentioned above. The bounce and the transit frequencies of electrons are much higher than that of ions, resulting in negligible contribution to the kinetic resonance

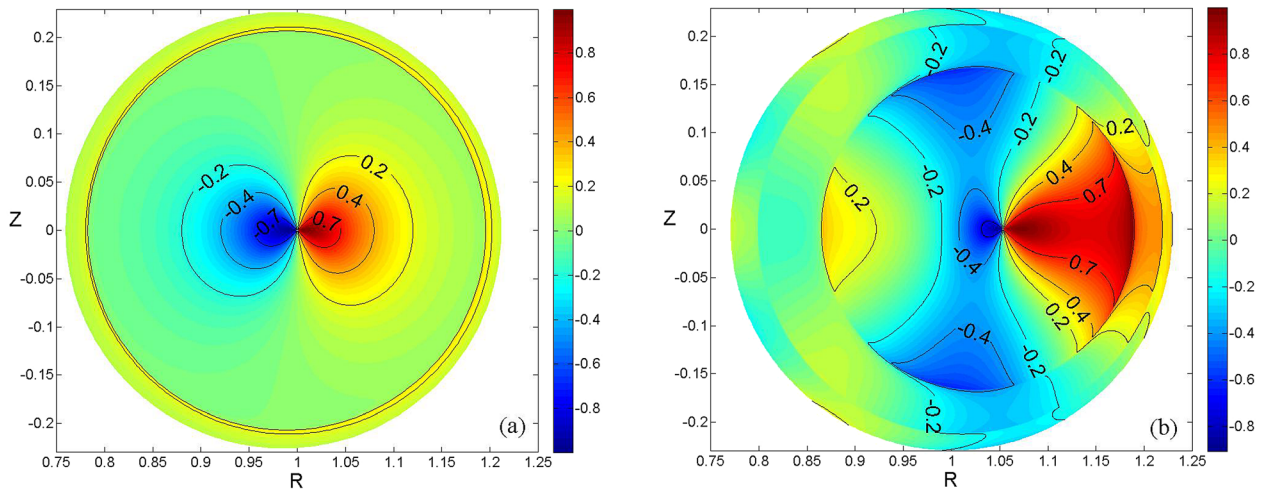


FIG. 2. The two-dimensional plots of the perturbed radial displacement of the fluid RWM. The maximum absolute value of the displacement is used to normalize the mode: (a) the  $n=6$  mode in RFP with  $F = -0.06$ ,  $\Theta = 1.58$ ,  $\beta_p = 0.17$ , and  $q(0) = 0.144$ , corresponding to the case of Fig. 1(a); (b) the  $n=1$  mode in tokamak with  $q(0) = 1.14$ ,  $q(a) = 3.68$ ,  $\beta = 0.01$ , and  $\beta_N = 2.85$ , corresponding to the case of Fig. 1(c). Shown is the real part of the displacement on a selected toroidal cross section. No plasma rotation is assumed.

effects on RWMs. The effect of the collisionality will be studied in future paper.

### A. Numerical results

In this subsection, we compare the behaviour of RWMs, including kinetic effects in the two configurations: the RFP and the tokamak with a circular cross-section. The parameters are taken to be similar to the RFX-mod,<sup>40</sup> with  $\varepsilon = a/R = 0.2295$ , the wall position  $b/a = 1.12$ , the electron density at the magnetic axis  $n_{e0} = 2.5 \times 10^{19}/\text{m}^3$ , and the temperature ratio between the thermal ions and electrons is  $T_i/T_e = 0.7$ . These parameters will be applied to all the following analyses, unless otherwise stated. The density profile is assumed as  $n_e(s) = n_{e0}(1 - s^2)$ . For the tokamak case, the pressure profile is modelled as  $P(s) = P_0(1 - s^2)^2$ . For the RFP case, we choose  $P = P_0(1 + a_{p1}s^2 + a_{p2}s^4 + a_{p3}s^6)$ . For the sake of simplicity, a uniform toroidal plasma rotation frequency is considered.

The growth rates of the  $n = 6$  RWM, as a function of the normalized plasma rotation frequency, is plotted in Fig. 3 for various  $\beta_p$  values in the RFP plasma. Figure 3(a) shows the computational results involving full kinetic effects of both trapped and passing particles. Four poloidal beta values are considered ( $\beta_p = 0.06, 0.11, 0.15, 0.17$ ). While increasing  $\beta_p$ , we kept the  $q(r)$  profiles nearly unchanged, with  $q(0) \approx 0.145$ ,  $q(a) \approx -0.01$ , and the reversal parameter  $F \approx -0.06$ . The pinch parameter  $\Theta$  has to be changed correspondingly in the range 1.5 to 1.58. The definition of  $F$ ,  $\Theta$ , and  $\beta_p$  can be found in Ref. 39. Figure 3(a) shows that, for the high  $\beta$  plasma, the RWM can be fully stabilizing at much slower plasma rotation than that predicted by the fluid theory.<sup>29</sup> Inclusion of the kinetic effects leads to a critical rotation frequency of  $\Omega \sim 0.04\omega_A$ , when  $\beta_p$  reaches 0.15 ( $\omega_A = \frac{B_0}{R_0\sqrt{\mu_0\rho_0}}$  is the Alfvén frequency at the magnetic axis.). With further increase of  $\beta_p$  up to 0.17, the RWM can be stabilized at even slower rotation of  $\Omega \sim 0.028\omega_A$ . The kinetic stabilization is mainly contributed by passing ions through the acoustic landau damping, as shown by Fig. 3(b).

The mode growth rates versus the normalized plasma rotation frequency  $\Omega/\omega_A$  are plotted in Fig. 3(b), for the case of  $\beta = 0.17$ . Four types of kinetic contributions are compared: (1) the full kinetic effects (dot-dashed line), (2) the precession resonance of trapped particles only (dotted line), (3) the precession and the bounce resonances (long dashed line), and (4) the transit resonance of passing particles alone (short dashed line). The result of the fluid theory (without kinetic effects, solid line) is also shown in the figure for the comparison. The figure clearly shows that the transit resonance plays a principle role, stabilizing the  $n = 6$  RWM with the slowest critical rotation speed (slower than that with the full kinetic effects). The trapped particle (both ions and electrons) precession resonance alone does not fully stabilize the mode. The precession resonance combined with the bounce resonance do not stabilize the mode either. Figure 3(b) also shows that the critical flow velocity for the mode stabilization by full kinetic effects ( $\Omega/\omega_A \approx 0.028$ ) is larger than that by transit resonance only ( $\Omega/\omega_A \approx 0.02$ ). This implies that the contributions from different kinetic resonances may play opposite role and slightly cancel each other.

Compared to the RFP plasmas, the behaviours of RWMs in tokamaks are rather different. Figure 4(a) plots the  $n = 1$  RWM growth rates, as a function of the normalized plasma rotation frequency  $\Omega/\omega_A$ , for circular cross section tokamak plasmas, where the full kinetic effects are taken into account. Two different equilibria are presented: (1) the first case with  $q_0 = 1.13$ ,  $q_a = 1.64$ , and  $\beta = 0.02$  ( $\beta_N = 2.68$ ), shown by the solid line. In this equilibrium, there is no mode rational surface inside the plasma. We find that the RWM is current drive. The kinetic effects cannot stabilize the mode with plasma rotation. (2) The second case has  $q_0 = 1.14$ ,  $q_a = 3.68$ , and  $\beta = 0.0105$  ( $\beta_N = 2.85$ ), shown by the dotted line. The RWM is pressure driven for this equilibrium (the mode is stable when  $\beta = 0$ ). The pressure scaling parameter  $C_\beta = (\beta_N - \beta_N^{no-wall})/(\beta_N^{ideal-wall} - \beta_N^{no-wall}) = 0.66$ . The kinetic effects stabilize the mode without plasma rotation or with a slow rotation at  $\Omega/\omega_A < 0.0048$ . The major contribution to the kinetic stabilization comes from the precession resonance of trapped particles.

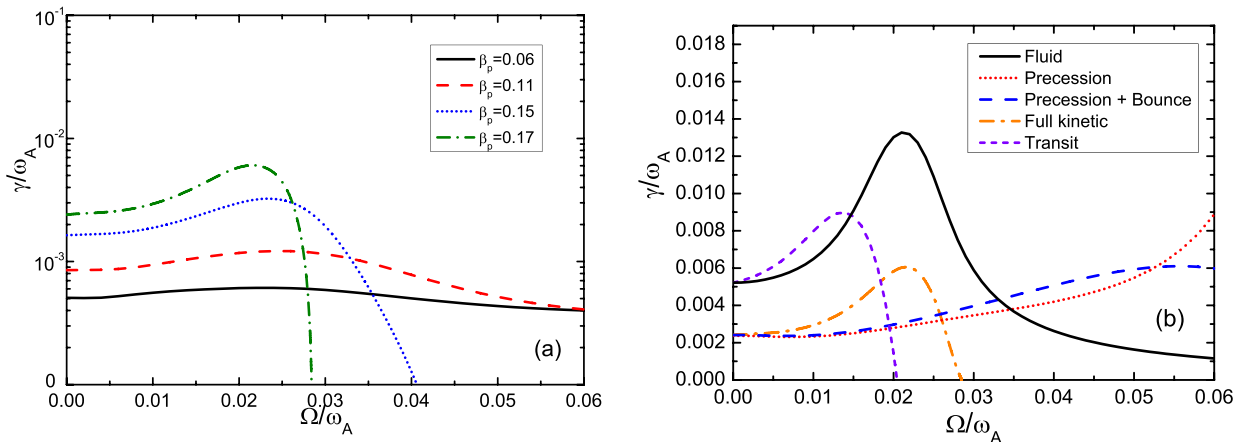


FIG. 3. The  $n = 6$  RWM growth rate  $\gamma$  versus the plasma rotation frequency  $\Omega$  in RFP plasmas: (a) the rotation frequency scan including full kinetic effects of both trapped and passing particles, with various  $\beta_p$  values  $\beta_p = 0.06$ (solid),  $0.11$ (dashed),  $0.15$ (dotted),  $0.17$ (dot-dashed). The other parameters are kept almost unchanged, with  $F \approx -0.06$  and  $q(0) \approx 0.145$ ; (b) the rotation frequency scan including different types of kinetic resonances, at  $\beta_p = 0.17$ . The  $\gamma$  and  $\Omega$  values are normalized by the Alfvén frequency  $\omega_A$  in the plasma center.

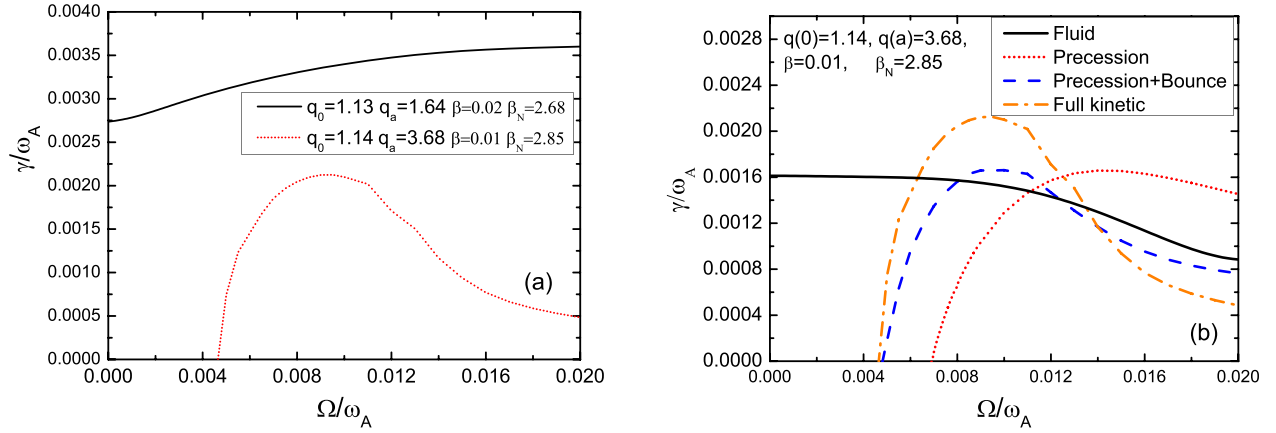


FIG. 4. The  $n = 1$  mode growth rate versus the plasma rotation frequency for tokamak equilibria: (a) the rotation scan including the full kinetic effects of both trapped and passing particles, for two equilibria; (b) the rotation scan for the  $q(a) = 3.68$  case, comparing contribution from various kinetic effects, as well as the fluid theory prediction.

Figure 4(b) shows the mode growth rates versus the rotation frequency, taking into account different kinetic effects for the pressure driven tokamak RWM (corresponding to the case shown by the dotted line in Fig. 4(a)). Here the dot-dashed line corresponds to the full kinetic effects, showing that the full stabilization can be achieved in the frequency range of  $\Omega/\omega_A \approx 0.0 - 0.0048$ . The dotted line corresponds to the case, where only the precessional resonance of trapped particles is considered. The dashed line presents the case, where both the precession and the bounce resonances of trapped particles are taken into account. The result of the fluid theory is also plotted (solid line). The comparison shows that the trapped particle precession resonance gives the principle contribution to the mode stabilization, at slow or vanishing plasma rotation. Again Fig. 4(b) shows that the full kinetic effects results in a narrower stable region in  $\Omega/\omega_A$ , than the precession resonance alone, implying a slight cancellation of the mode stabilizing effect between different kinetic resonances. As the rotation frequency  $\Omega$  increases beyond the above mentioned range, the mode becomes unstable again. With further increase of the plasma rotation frequency, the transit resonance starts to play a stabilizing role by the ion acoustic damping, and mode growth rate decreases. However, we do not find a full stabilization for this equilibrium.

## B. Physical understanding

Here, we perform detailed analysis of both fluid and drift kinetic potential energy perturbations. With the aim of improving the physical understanding, we consider the generalized dispersion relation<sup>20,41</sup>

$$\gamma \tau_w^* = - \frac{\delta W_\infty + \delta W_k}{\delta W_b + \delta W_k}, \quad (16)$$

where  $\delta W_\infty = \delta W_F + \delta W_{v\infty}$ ,  $\delta W_b = \delta W_F + \delta W_{vb}$ ,  $\delta W_{vb}$ , and  $\delta W_{v\infty}$  are the vacuum energy with an ideal wall at minor radius  $b$  and without the wall, respectively.  $\tau_w^*$  characterizes the wall time of a resistive wall.  $\delta W_F$  is the fluid energy component as given in Eq. (11),  $\delta W_k$  is the potential energy from

the kinetic resonance as presented in Eq. (15). The plasma inertial contribution is found to be small compared to other terms, and hence has been neglected in Eq. (16). All energy components are evaluated using the RWM eigenfunctions, obtained from the self-consistent computations. We note that, even though not fully corresponding to the self-consistent computation, Eq. (16) does approximately describe the RWM physics in the region of slow rotation velocity as we investigate here.

The kinetic energy  $\delta W_k$  consists of the resonant (imaginary) part and the non-resonant (real) part,  $\delta W_k = \delta W_k^{re} + i\delta W_k^{im}$ . It follows from Eq. (16) that the stabilization of the RWM requires the condition

$$\delta W_\infty \delta W_b + \delta W_k^{re} (\delta W_b + \delta W_\infty) + (\delta W_k^{re})^2 + (\delta W_k^{im})^2 > 0. \quad (17)$$

Generally, the imaginary part always gives a stabilizing effect. The real part can be either stabilizing or destabilizing effects. Figure 5 compares various energy components, normalized by the total driven energy  $\delta W_{\text{driven}} = -(\delta W_{\text{pre}} + \delta W_{\text{cur}})$  (the current driven plus the pressure driven energy components) of RWM, for the two configurations. Figure 5(a) is for the  $n = 6$  RWM in the RFP plasma and (b) is for the  $n = 1$  mode in the tokamak plasma. Each figure has several groups of columns. The first column shows the total driving energy components (current driven and pressure driven). The second column represents the stabilizing energy components, including the magnetic field line bending term  $\delta W_{mb}$ , the magnetic compressibility term  $\delta W_{mc}$  and the vacuum magnetic energy term  $\delta W_{v\infty}$ . The third column shows the vacuum energy  $\delta W_{vb}$ , with an ideal wall located at the minor radius  $b$ . This is also a stabilizing term and, together with  $\delta W_F$ , determines the critical wall position for the ideal kink instability. The fourth column in each group shows  $\delta W_\infty$  and  $\delta W_b$  as defined in Eq. (16). The last two columns represent the real and imaginary parts of  $\delta W_k$ , respectively.

Figure 5(a) shows the energy comparison for RFP plasmas, where only the ion transit resonances are considered.

There are three groups of columns. Group (1) is for an equilibrium with  $\beta_p = 0$ ,  $F = -0.063$ ,  $\Theta = 1.454$ ,



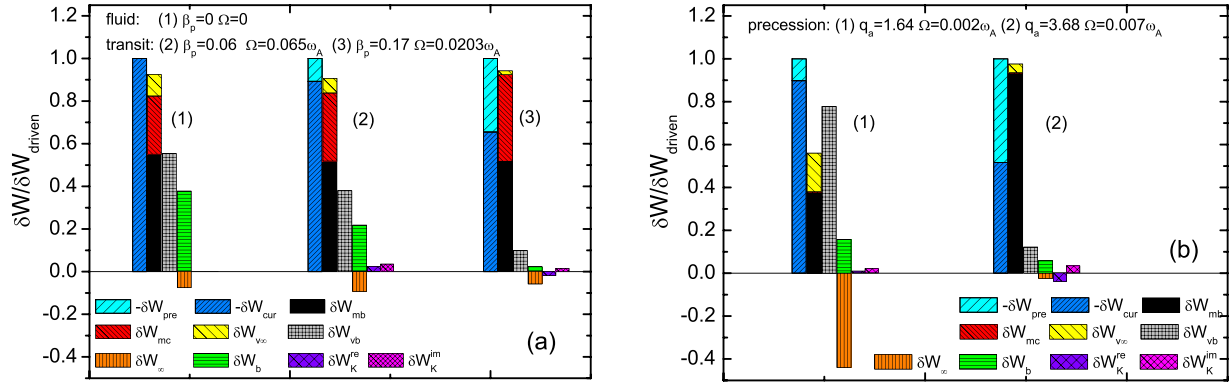


FIG. 5. The potential energy components of the RWM, as defined in Eqs. (11)–(14) and normalized by the driven terms  $\delta W_{\text{driven}} = -(\delta W_{\text{pre}} + \delta W_{\text{cur}})$ , are calculated at various plasma rotation velocities for (a) the  $n=6$  mode in RFP plasmas with  $F \approx -0.06$ ,  $q(0) \approx 0.145$ , including the mode resonance with transit frequency of passing ions only, at three chosen  $\beta_p$  values:  $\beta_p = 0.0$ ,  $0.06$ , and  $0.17$ ; (b) the  $n=1$  mode in tokamak plasmas with  $q(0) = 1.13$ ,  $q(a) = 1.64$ ,  $\beta = 0.02$ ,  $\beta_N = 2.68$  (group 1), and  $q(0) = 1.14$ ,  $q(a) = 3.68$ ,  $\beta = 0.01$ ,  $\beta_N = 2.85$  (group 2). The mode resonance with precessional drifts of trapped ions and electrons are considered.

$q(0) = 0.147$ , and  $q(a) = -0.0104$ . Neither plasma rotation nor kinetic effects are included. Due to vanishing equilibrium pressure, only the current driven energy component appears. Since the driven energy prevails in the balance between the first and second columns, the no-wall ideal kink mode is unstable, and hence the RWM is unstable. The fourth column shows a negative  $\delta W_\infty$  and a positive  $\delta W_b$ , agreeing with the RWM instability following Eq. (16).

Group (2) is for an equilibrium with middle range  $\beta_p$ ,  $\beta_p = 0.064$ , and  $F = -0.063$ ,  $\Theta = 1.499$ ,  $q(0) = 0.145$ ,  $q(a) = -0.010063$ . This case corresponds to the solid curve in Fig. 3(a). The flow velocity of  $\omega_E/\omega_A = 0.065$  is assumed in the computation, at which the kinetic resonances contribute a maximal value of  $\delta W_k$ , along the whole velocity range considered in Fig. 3(a). The pressure driven energy in this case is only a small fraction of total driven term  $\delta W_{\text{driven}}$ . The current driven is still the dominant destabilizing mechanism. The computed  $\delta W_\infty$  and  $\delta W_b$  have rather large values. The kinetic energy component  $\delta W_k$  has small real and imaginary parts, being not sufficient to stabilize the mode.

Group (3) is for a high  $\beta$  RFP plasma, with  $\beta_p = 0.17$ , and  $F = -0.062$ ,  $\Theta = 1.565$ ,  $q(0) = 0.144$ ,  $q(a) = -0.0094$ , corresponding to the dot dashed line in Fig. 3(a). Included are the effects of the transit resonance of passing ions on the  $n=6$  mode, at the flow velocity  $\Omega/\omega_A = 0.0203$ , which is near the marginal instability. The fraction of the pressure driven energy is significantly increased in this case, compared with the case of  $\beta = 0.06$ . The magnetic compressional term becomes slightly larger. Both  $\delta W_\infty$  and  $\delta W_b$  become smaller than that in groups (1) and (2). The kinetic energy components, both  $\delta W_k^{\text{re}}$  and  $\delta W_k^{\text{im}}$ , play a stabilizing role and lead to a very small growth rate—the mode is nearly marginally stable. With further increasing  $\Omega/\omega_A$ , we obtain a completely stable RWM.

Figure 5(b) is the counterpart plot for tokamaks. The group (1) is for an equilibrium with  $q(a) = 1.637$ ,  $q(0) = 1.13$ , and  $\beta = 0.02$  ( $\beta_N = 2.68$ ), corresponding to the solid line in Fig. 4(a) at  $\Omega/\omega_A = 0.002$ , where the kinetic effect contributes a maximal value of  $\delta W_k$  along the whole range of the velocity. In this equilibrium, all rational surfaces of the  $n=1$  modes are located outside the plasma.

The RWM is a current driven mode—the pressure driven energy component is much smaller than the current driven component. The total stabilizing components are also smaller than the current driven component. The resulting  $\delta W_\infty$  is rather large. Moreover,  $\delta W_{vb}$  and  $\delta W_b$  are much larger than that in the second group. The kinetic energy  $\delta W_k$ , being roughly proportional to the equilibrium pressure, is rather small and cannot stabilize the mode. In tokamak plasmas, due to the strong toroidal magnetic field, the magnetic compression energy  $\delta W_{mc}$  is very small and almost invisible in the figure.

Group (2) is for a tokamak plasma with  $q(a) = 3.68$ ,  $q(0) = 1.14$ , and  $\beta = 0.0105$  ( $\beta_N = 2.85$ ), corresponding to the dotted curve in Fig. 4(b), which describes the effect of precessional resonance of trapped particles on the  $n=1$  mode. The rotation frequency  $\omega_E/\omega_A = 0.007$  is chosen near the critical value for the marginal stability. The first column in this group shows a large pressure driven fraction, contributing almost half of the driving energy. In fact the RWM is a pressure driven mode for this equilibrium. The stabilizing column from the fluid terms,  $\delta W_{mb} + \delta W_{v\infty}$ , is larger than that of group (1), and leads to a smaller  $\delta W_\infty$ . The vacuum energy  $\delta W_{vb}$  is smaller as well, leading to a smaller  $\delta W_b$ . The kinetic energy  $\delta W_k$  contributes sufficiently strong stabilizing effect, such that the mode is marginally stable. Further decreasing the plasma rotation  $\Omega$ , the mode can be completely stabilized as showed in Fig. 4(b).

Figure 5 demonstrates a common feature of RWM for both configurations: the kinetic stabilization requires a large fraction of the pressure driven energy component. In fact, even with large fraction of  $\delta W_{\text{pre}}$ , the drift kinetic energy is still small compared to other energy components. The stabilization condition in Eq. (17) indicates that only with very small  $\delta W_\infty$  or  $\delta W_b$  (which leads to the first destabilizing term  $(\delta W_b \delta W_\infty)$  being small), the kinetic effects can play a significant role for the RWM stability. Numerical results from Fig. 5 show that having small fluid energy components  $\delta W_b$  or  $\delta W_\infty$  is indeed the critical ingredient for the drift kinetic damping of the RWM. As is well-known,  $\delta W_\infty \rightarrow 0$  implies the marginal RWM stability (or the marginal external ideal kink stability without wall), and  $\delta W_b \rightarrow 0$  is the

marginal ideal kink stability with ideal wall at  $b$  ( $b$  is near the critical wall position).

In RFPs, almost in all the cases, stabilization occurs only when  $\delta W_b$  is very small, i.e., near the critical wall position. Increasing the equilibrium pressure and/or moving the resistive wall away from the plasma surface can reduce  $\delta W_b$ . Fig. 5(a) compares the three RFP results with increasing different  $\beta_p$  values, but with almost the same  $q(r)$  profiles. More detailed analysis shows that increasing the equilibrium pressure decreases the perturbed fluid displacement in the normal direction,  $\xi_n$ , near the plasma edge, and increases the other two components along the tangential direction; this causes smaller normal magnetic perturbation  $b_n$  at plasma-vacuum interface. It turns out that the perturbed vacuum magnetic energy  $\delta W_{vb}$  (proportional to  $b_n^2$ ) becomes smaller, and so does  $\delta W_b$ .  $\delta W_b \rightarrow 0$  implies the marginal stability of the external kink with an ideal wall. This is where the mode stability can become more sensitive to any type of dissipations (or excitations). We find the same behaviour in tokamaks, as in the RFP plasmas, if we keep the  $q(r)$  invariant while changing the  $\beta$  value.

In tokamaks, both  $\delta W_b \rightarrow 0$  and  $\delta W_\infty \rightarrow 0$  can occur. When  $\beta_N$  just above  $\beta_N^{\text{no-wall}}$ ,  $\delta W_\infty$  is very small, which implies the marginal stability of RWM. While as  $\beta_N$  going up to be close to the  $\beta_N^{\text{ideal-wall}}$ ,  $\delta W_b$  is very small, which implies the marginal stability of the ideal kink mode. In both case, the kinetic effects can be more important on the RWM stabilization. The tokamak equilibrium with larger  $q(a)$  implies that, for the same plasma current, the toroidal magnetic field is stronger. And the plasma is generally more resistant to the “kink” instability. Therefore, a plasma with a larger  $q(a)$  needs larger pressure driven energy to become kink unstable. In fact, it is found that the second group, with  $q(a)=3.68$ , provides a stronger magnetic bending and smaller  $\delta W_{vb}$ , than the first group with  $q(a)=1.67$ . The smaller  $\delta W_{vb}$  for the second group is associated with the smaller magnetic perturbation at the plasma surface. For the tokamak equilibria considered here, a larger  $q(a)$  leads to a higher no-wall  $\beta$  limit, thus to a larger pressure driven potential energy  $\delta W_{\text{pre}}$ . Consequently, it leads to a small  $\delta W_b$ , and

the mode becomes easy to be stabilized by the kinetic effects. For  $1 < q(a) < 2$ , we observe only current driven RWMs, which cannot be stabilized by the kinetic effects of thermal particles.

Next, we try to understand why the precessional resonance of trapped particles, at very slow plasma rotation, can give the RWM stabilization in tokamaks, but not in RFPs. Figures 6(a) and 6(b) plot various frequencies, entering the resonance operator  $\lambda_{m,l}$  of Eq. (10), for RFP and tokamak plasmas, respectively. The flux surface averaged precession drift frequency  $\omega_d$ , the bounce frequency  $\omega_b$  of trapped particles (ions and electrons), the resonance ion transit frequency term  $(m-nq)\omega_p$  ( $\omega_p$  is the transit frequency), and the diamagnetic drift frequency  $\omega_*$  ( $\omega_* = \omega_{*N} + \omega_{*T}$  includes both density gradient drift and temperature gradient drift) are plotted as a function of the normalized radial coordinate  $s$ .

In both Figures 6(a) and 6(b), the dotted curves present the precession frequencies of trapped electrons  $\omega_{de}$  (the precession frequency of trapped ions is defined as  $\omega_{di} = -(T_i/T_e)\omega_{de}$ , and plotted as dual-dot-dashed line). Note that in the tokamak configuration, the scale lengths of the magnetic curvature and gradient are in order of  $O(1/R)$ , which is one order of  $O(\epsilon)$  smaller than that in RFP, which is in the order of  $O(1/a)$ . In fact, Fig. 6 demonstrates that the averaged precession frequency (over the flux surface)  $\omega_d$  is near zero in the tokamak, and is around 0.005–0.01 in the RFP configuration. For very small rotation frequency  $\Omega \approx 0$ , the ion and electron contributions of the  $\omega_d$  resonance, to the imaginary part of  $\delta W_k$  ( $\delta W_k^{\text{im}}$ ), have opposite signs, and the two contributions almost cancel each other. Therefore, the precessional drifts mostly contribute to the real part of  $\delta W_k$  ( $\delta W_k^{\text{re}}$ ). As the  $\Omega$  ( $>0$ ) value increases, the trapped electrons start to play a more important role. The ratio  $\omega_*/\omega_d$  is significant in determining the integrated value of the resonance operator  $\lambda_{m,l}$ . The following three points may provide the reasons why the trapped particles play different roles in tokamaks and in RFPs. First, the fraction of the trapped particle in RFPs is smaller than that in tokamaks. This is particularly true near the low field side edge of the plasma. Second, the ratio  $\omega_*/\omega_d$  is much larger in tokamaks, than that in RFPs,

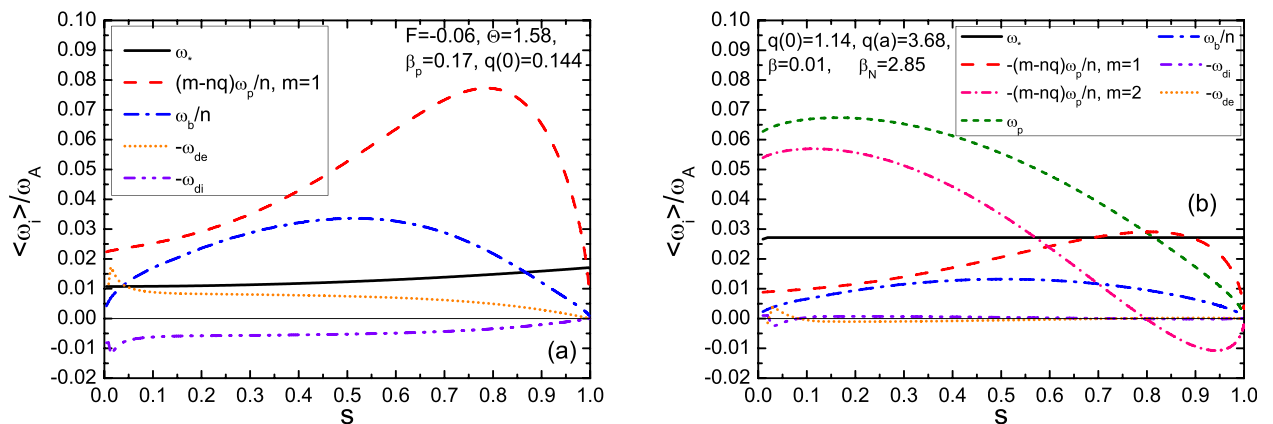


FIG. 6. The radial profiles of various frequencies of trapped and passing thermal particles, averaged over the velocity space and over the poloidal angle. The diamagnetic frequency ( $\omega_*$ ), the precession frequencies of trapped ion ( $\omega_{di}$ ) and electron ( $\omega_{de}$ ), the bounce frequency of trapped ions ( $\omega_b/n$ ), as well as the resonant transit frequencies  $(m-nq)\omega_p/n$  of passing ions are plotted for (a) the RFP case with  $m=1$ ,  $n=6$ ,  $F=-0.06$ ,  $\Theta=1.58$ ,  $\beta_p=0.17$ ,  $q(0)=0.144$ , and (b) the tokamak case with  $m=1, 2$ ,  $n=1$ ,  $q(0)=1.14$ ,  $q(a)=3.68$ ,  $\beta=0.0105$ ,  $\beta_N=2.85$ .

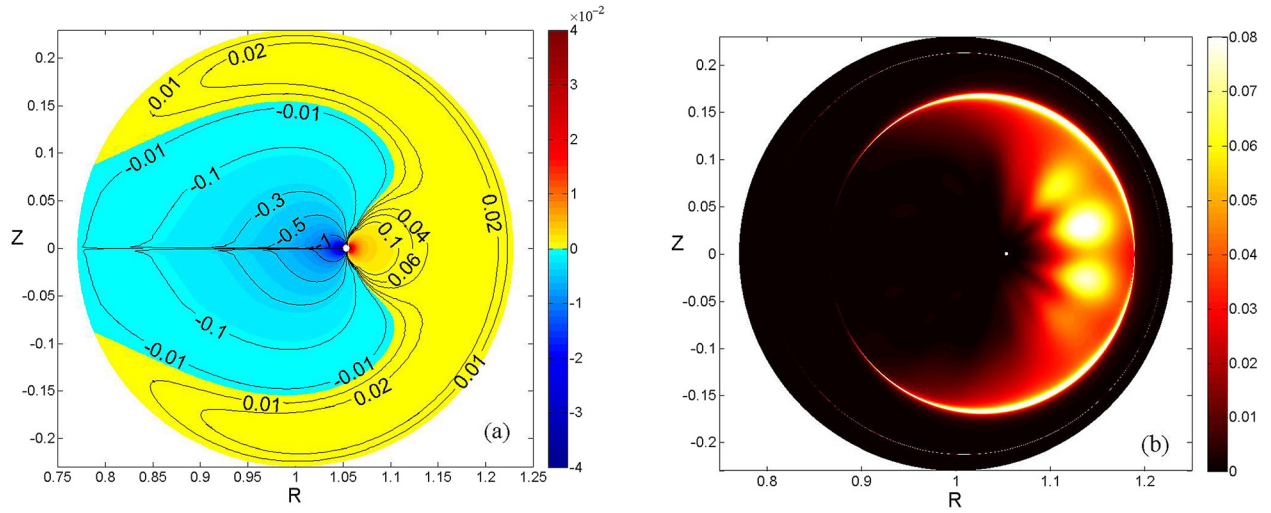


FIG. 7. The 2D plots in the RZ-plane, of (a) the precession frequency  $\omega_{de}$  of trapped electrons, averaged over the velocity space, and (b) the  $|\delta W_k|$  for the  $n=1$  marginally stable RWM, in the presence of the precessional resonance of trapped ions and electrons, for a tokamak plasma with  $\Omega=0.007\omega_A$ ,  $q(0)=1.14$ ,  $q(a)=3.68$ ,  $\beta=0.01$ , and  $\beta_N=2.85$ . The  $|\delta W_k|$  is normalized by  $\delta W_{\text{driven}}$ . The value of  $\omega_{de}$  is normalized by  $\omega_A$ .

resulting in a larger value of  $\delta W_k$ . Finally, the tokamak plasma is characterized by a stronger toroidal coupling, where several poloidal harmonics grow together, with comparable amplitude. Each poloidal harmonic can be in resonance with particle precessions. The RWM in the RFP plasma, on the contrary, has a weak toroidal coupling, and only mode  $m=1$  gives the dominant contribution, due to the precessional resonance, to the kinetic energy. Therefore, the trapped particle precessional drifts can stabilize the RWM in tokamaks for very plasma slow rotation, starting from  $\Omega=0$ , while the same drifts play a minor role in the stabilization of the mode in RFPs, in the frequency range  $\Omega/\omega_A \sim \omega_d \approx 0.005-0.01$ .

The particle phase space averaged precession frequency, for a tokamak plasma, is plotted in Fig. 7(a) in the toroidal cross section. It is interesting to notice the change of sign of  $\omega_d$ , from the low field side to the high field side. Moreover,

the magnitude of  $\omega_d$  stays near zero in a large region. In fact, we find that the precessional resonance gives the largest contribution to  $\delta W_k$  in the yellow area, as shown by Fig. 7(b).

The dashed line in Fig. 6(a) shows the resonant transit frequency  $(m-nq)\omega_p$  for the  $m=1$ ,  $n=6$  mode in the RFP plasma. In the area of minor radius  $s \approx 0.2-0.3$ , corresponding to  $\Omega/\omega_A \approx 0.025-0.035$ , the transit resonance starts to give a significant contribution to  $\delta W_k$ , leading to the stabilization of the mode. With further increase of the flow velocity, the kinetic contribution  $\delta W_k$  becomes more important, and the mode becomes fully stable. Figure 8(a) shows the amplitude of the kinetic energy  $|\delta W_k|$  distribution in the toroidal cross section. The largest contribution comes from the low field side near the plasma core region (the bright area). This is because the perturbed particle Lagrangian  $H_L$ , which is well represented by the  $\kappa \cdot \xi_\perp$  term, has the maximum in this area, as shown by Fig. 8(b). The dominant contribution

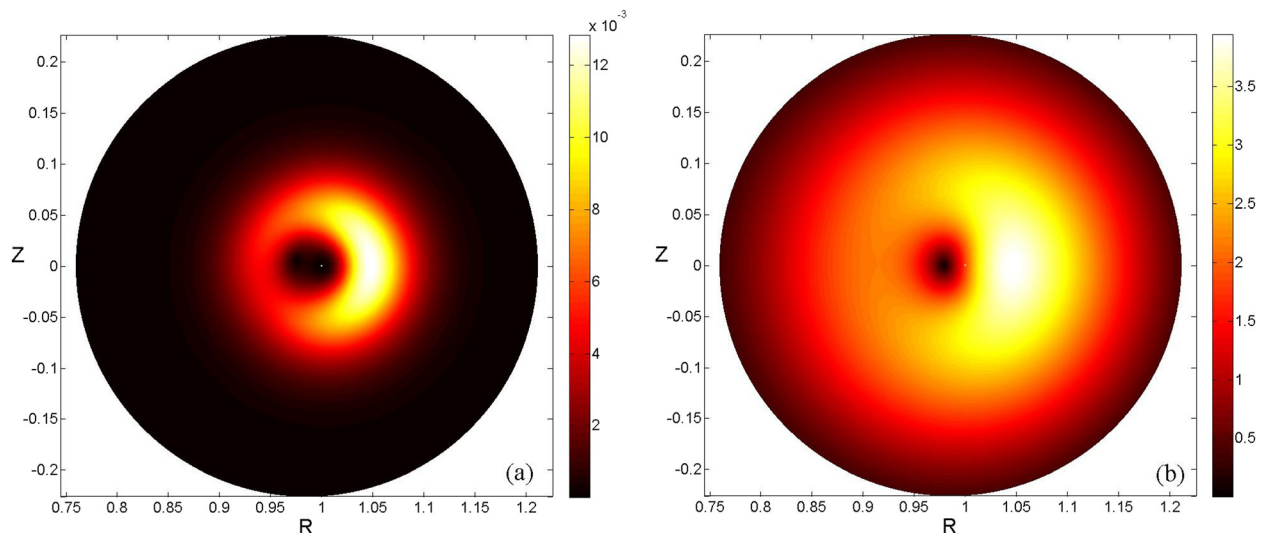


FIG. 8. The 2D plots in the RZ-plane, of (a)  $|\delta W_k|$  for the  $n=6$  marginally stable RWM, including the transit resonance of passing ions alone, and (b) The value of  $|\kappa \cdot \xi_\perp|$  (in arbitrary unit), for a RFP plasma with  $\Omega=0.0203\omega_A$ ,  $F=-0.06$ ,  $\Theta=1.58$ ,  $\beta_p=0.17$ , and  $q(0)=0.144$ .  $|\delta W_k|$  is normalized by  $\delta W_{\text{driven}}$ .

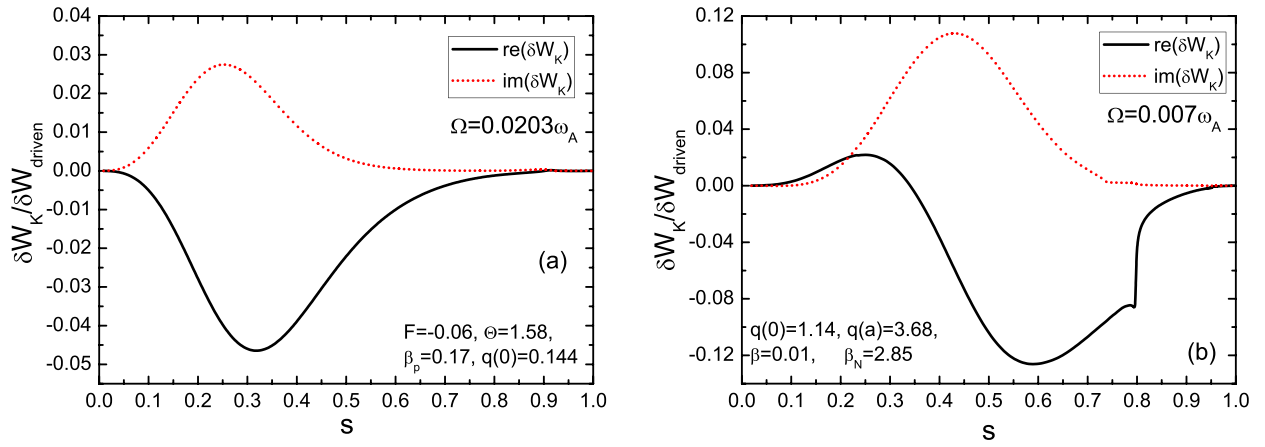


FIG. 9. The radial distribution of the real and imaginary parts of  $\delta W_k$ , integrated over the phase space and the poloidal angle, for (a) the  $n=6$  marginally stable RWM in the RFP plasma, where the mode resonance with the transit frequency of passing ions alone is included, with  $\Omega=0.0203\omega_A$ ; (b) the  $n=1$  marginally stable RWM in the tokamak plasma, in the presence of the mode resonance with precessional drifts of trapped ions and electrons.

to  $\delta W_k$  comes from the  $m=1$  and the  $l=0$  harmonic in Eq. (15). We notice that the bounce frequency  $\omega_b/n$  in that area is also close to the transit one, and should in principle also give contribution to the kinetic energy. However, our computations reveal that the bounce resonance gives minor influence on the mode stability. This may be due to the small fraction of trapped particles (compared to passing particles), as well as the fact that the  $l=1$  bounce harmonic in the Lagrangian  $H_L$  is less important than the  $l=0$  harmonic.

Figure 9(a) plots the radial profiles for both the real and imaginary parts of the kinetic energy  $\delta W_k$ , due to the transit resonance at  $\Omega/\omega_A=0.02$ , for the RFP plasma. These radial profiles are obtained as a result of the integration along the poloidal angle, for the energy distribution shown in Fig. 8(a). Figure 9(a) confirms that both the real and imaginary parts of  $\delta W_k$  reach their peak values in the range of  $s=0.2-0.3$ .

For the tokamak equilibrium with  $q(a)=3.68$ ,  $q(0)=1.14$ , and  $\beta=0.0105$ , the most important resonant transit frequencies, for the  $n=1$  RWM, are the  $m=1$  and  $m=2$  harmonics, presented by the dashed and dot-dashed curves, respectively, in Fig. 6(b). The transit resonance requires a much larger plasma rotation than the precessional resonance. For this equilibrium, we did not find the full stabilization of the RWM with the transit resonance.

Figure 9(b) plots of the radial distribution of both the real and imaging parts of the kinetic energy  $\delta W_k$  (integrated over the magnetic surface), contributed by the precessional resonance of trapped particles. The largest kinetic contribution appears in the range of minor radius, where  $\omega_d \approx 0$ .

## V. NON-PERTURBATIVE VERSUS PERTURBATIVE RESULTS

In this work, we have adopted the self-consistent approach, where the drift kinetic effects are coupled to the MHD equations in a non-perturbative manner. Another approach is the perturbative one,<sup>42,43</sup> where the fluid part is considered as the lowest order term, and the kinetic part as the next order. The drift kinetic energy is calculated using the eigenfunction of the fluid RWM or the marginally stable ideal kink mode (with an ideal wall). The non-perturbative approach allows a self-

consistent modification of the RWM eigenfunction, due to the kinetic effects. Furthermore, the complex eigenvalue of the RWM is obtained self-consistently by solving the hybrid eigenmode equations, where the mode frequency dependent kinetic resonance operators are taken into account via the perturbed kinetic pressure tensor.

In the following, we give an example comparing these two approaches. We use the same tokamak equilibrium as for Fig. 1(d), with  $q(0)=1.13$ ,  $q(a)=1.64$ , and  $\beta=0.02$  which is ideal for the study of the two approaches on the  $n=1$  RWM since there is no mode resonant surface inside the plasma, and hence no singular behaviour appears in the mode eigenfunction. The plasma rotation  $\Omega=0$  is assumed.

Figure 1(d) (Sec. III) showed the radial profiles of the eigenfunctions  $\xi_n$ , obtained by the fluid theory. The  $m=1$  harmonic is dominant, with the  $m=2$  harmonic having relatively smaller amplitude. Shown in Fig. 10 is the eigenfunction for  $\xi_n$ , obtained by the selfconsistent approach. Clearly, the amplitude of the  $m=2$  harmonic is largely increased due to the kinetic effects, and in fact becomes one of the dominant modes.

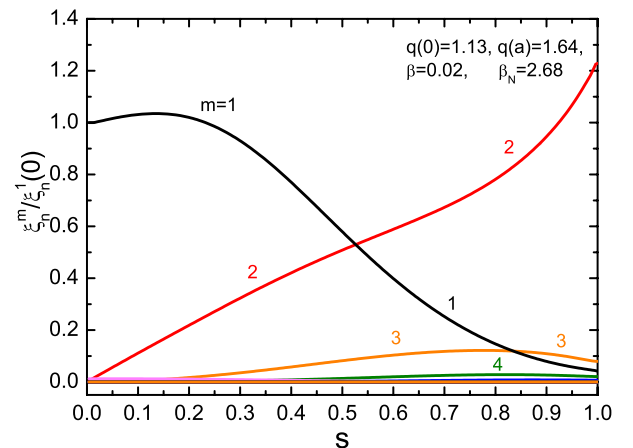


FIG. 10. The radial profiles of the poloidal Fourier harmonics of perturbed radial displacement, for the self-consistently computed  $n=1$  RWM including the full kinetic effects, for the tokamak equilibrium with  $q(a)=1.64$ . A straight field line coordinate system is used. No plasma rotation is assumed.



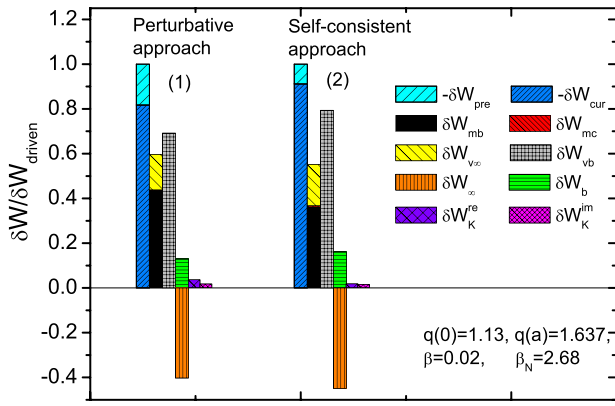


FIG. 11. The potential energy components, as defined in Eqs. (11)–(14) and normalized by the driven terms  $\delta W_{\text{driven}} = -(\delta W_{\text{pre}} + \delta W_{\text{cur}})$ , are plotted for the  $n = 1$  RWMs, for the  $q(a) = 1.64$  tokamak equilibrium, where the full kinetic effects are included. Group (1) adopts the perturbative approach with the fluid RWM eigenfunction. Group (2) is calculated in the self-consistent approach. No plasma rotation is assumed.

Consequently, the energy components normalized by  $\delta W_{\text{driven}}$  and calculated from the two different eigenfunctions, are also different as shown in Fig. 11. Two groups of the energy components are plotted. The first one comes from the perturbative approach, where the energy components are computed using the eigenfunction of the fluid RWM. The second group of energy is computed using the RWM eigenfunction obtained from the self-consistent approach. In the second group, the current driven term contributes a larger fraction, due to the kinetic modification of the mode eigenfunction. The kinetic energy from the two approaches, though different, is still much smaller than the fluid energy  $\delta W_{\infty}$ . Therefore, for this equilibrium, the kinetic effects cannot stabilize the RWM following either approach. The variation of the mode eigenfunction, as well as the energy components, does not result in a qualitative difference in the mode eigenvalues (perturbative approach:  $(\gamma + i\omega_r)/\omega_A = 2.51 \cdot 10^{-3} - i3.55 \cdot 10^{-4}$ ; self-consistent approach:  $2.74 \cdot 10^{-3} - i2.98 \cdot 10^{-4}$ ). Because  $\delta W_k \ll \delta W_{\infty}$ , it is understandable that the perturbative approach should not give large discrepancy in the mode eigenvalue, compared to the self-consistent approach.

The above analysis indicates that when RWM is unstable and far from the marginal stability condition, the fluid energy components ( $\delta W_{\infty}$ ,  $\delta W_b$ ) are much larger than the kinetic energy  $\delta W_k$ . In this case, the results from the two approaches do not seem to show a large difference in the mode growth rate. However, when  $\delta W_{\infty}$  and  $\delta W_b$  are almost comparable with  $\delta W_k$ , for example when the RWM is near the marginal stability, or when the plasma rotation is included, the perturbative approach may lead to a large discrepancy (even qualitative) from the non-perturbative one. Some of the previous works have shown this point,<sup>32,47</sup> and we will further investigate it in detail.

## VI. SUMMARY AND DISCUSSIONS

We have studied the drift kinetic effects on the RWM for both RFP and tokamak plasmas, using the toroidal MHD-kinetic hybrid code MARS-K. In MARS-K, the kinetic resonant effects are incorporated into MHD formulation via the perturbed kinetic pressure tensor. The unknown mode growth rate and the mode eigenfunction are self-consistently obtained by solving the hybrid eigenmode equations. A new module for computing various potential energy components, based on the kinetic-modified RWM eigenfunction, has been developed and integrated into MARS-K. The module helps to make comprehensive energy analyses and to obtain in-depth physics understanding.

Our studies reveal that the kinetic dissipations on the RWM instability, in RFPs and tokamaks, are due to different kinetic mechanisms, resulting in different stabilizing conditions for the mode in the two systems. The differences in the RWM behavior are directly linked to the characteristics of the two different magnetic configurations. The RFP configuration is characterized by the low  $q$  profile, with the poloidal magnetic field ( $B_z$ ) being in the same order as the toroidal field ( $B_\phi$ ), and with a toroidal field reversal in the plasma edge. The tokamak plasma has a stronger toroidal field  $B_\phi$ , being the order of  $1/\epsilon$  greater than  $B_z$ , and with  $B_\phi \propto 1/R$ . We briefly summarize the comparison results in the following Table I.

A comparison of various potential energy components in both configurations demonstrated certain common features,

TABLE I. Comparison between the RFP and the tokamak plasmas on the RWM stability, with the inclusion of kinetic resonances.

RFP	Tokamak
RWMs are current driven modes.	RWMs are often pressure driven modes.
All RWMs are “non-resonant” modes.	RWMs can be either “resonant” or “non-resonant” modes.
Weak toroidal coupling, only one poloidal harmonic dominant	Strong toroidal coupling, multiple poloidal harmonics grow together with comparable amplitudes
Almost no ballooning character in the mode structure	Usually clear ballooning character in the mode structure
Internal non-resonant modes can be stabilized by the plasma rotation with the frequency being in the ion acoustic range for high $\beta$ plasmas.	Pressure driven RWM can be stabilized at very slow plasma rotation ( $\Omega < 0.5\% \omega_A$ ), or even without rotation.
Kinetic stabilization is mainly due to the mode resonance with transit frequency of passing particles (ion acoustic Landau damping).	Kinetic stabilization at slow velocity is mainly due to the mode resonance with precessional drifts of trapped particles.
The precessional resonance of trapped particles can not stabilize the RWM.	Current driven modes can not be stabilized by the precessional resonance.

namely that the kinetic stabilization requires a large fraction of the pressure driven energy component. Furthermore, decreasing the energy components  $\delta W_b$  and/or  $\delta W_\infty$ , is actually a critical ingredient in bringing the kinetic energy component to play an important role in the mode stabilization. In RFPs, we found that the stabilization often occurs when  $\delta W_b \rightarrow 0$ . Increasing the equilibrium pressure and/or moving the resistive wall away from the plasma surface can reduce  $\delta W_b$ . The analysis found that increasing the plasma  $\beta$  leads to the decrease of the normal component of the displacement, as well as the normal perturbed magnetic field at plasma edge, which in turn reduce the perturbed vacuum energy  $\delta W_{vb}$ , thus reduce  $\delta W_b$ . In tokamaks, both  $\delta W_b \rightarrow 0$  and  $\delta W_\infty \rightarrow 0$  can occur, implying that the drift kinetic effects can be more important near the no-wall or ideal-wall beta limits. Moreover, a tokamak equilibrium with larger  $q(a)$  implies that, for the same plasma current, the toroidal field is stronger. Such plasma is more resistant to the kink instability, thanks to the larger magnetic bending energy. In our case, a larger  $q(a)$  also leads to a higher no-wall  $\beta$  limit, thus a larger pressure driven potential energy  $\delta W_{pre}$ . All these factors explain that, with a larger  $q(a)$ , it is easier to stabilize the RWM by kinetic effects.

In this study, we use the wall position at  $b/a = 1.12$  for all of the calculations. Therefore, the effects of the wall position on the kinetic stabilization have not been discussed. Actually, this effect is also an important ingredient for the RWM stability because it is directly related to the vacuum energy component  $\delta W_{vb}$ . This study will be presented elsewhere.<sup>44</sup>

A uniform flow velocity has been assumed in this study. Compared to the shear flow, this assumption may lead to certain quantitative discrepancies. In tokamak plasmas, if the mode rational surfaces are located inside the plasma, the stability may be more sensitive to the profile of the flow velocity. We leave this issue for the future work. Another assumption is the circular cross section for the tokamak plasmas, in order to make a comparison with the circular RFP plasma. We believe that the physics for the shaped tokamak plasmas is similar to the pressure driven case that we have studied in the present work.

The comparison between non-perturbative and perturbative approaches has been made and the preliminary results have been obtained by investigating one simple example for the tokamak equilibrium. The investigation indicates that when the RWM is unstable and far from the marginal stability, although a large modification of the RWM eigenfunction by the kinetic effects can appear, the perturbative approach only gives a small quantitative discrepancy in the mode eigenvalue, compared to the non-perturbative approach. However, in many other situations that we investigated, in particular, when RWM is near the marginal stability, or in the presence of plasma rotation, the two approaches can lead to rather large, even qualitative, discrepancies. The discrepancies were also pointed out by other results in several works.<sup>32,47</sup> Further investigations and the detailed discussions on the physical mechanism causing the discrepancies between two approaches will be pursued and presented in the future work.

- <sup>1</sup>R. Aymar, V. A. Chuyanov, M. Huguet, Y. Shimomura, ITER Joint Central Team, and ITER Home Teams, *Nucl. Fusion* **41**, 1301 (2001).
- <sup>2</sup>F. Troyon, R. Gruber, H. Saurenmann, S. Semenzato, and S. Succi, *Plasma Phys. Controlled Fusion* **26**, 209 (1984).
- <sup>3</sup>A. M. Garofalo, A. D. Turnbull, M. E. Austin, J. Bialek, M. S. Chu, K. J. Comer, E. D. Fredrickson, R. J. Groebner, R. J. La Haye, L. L. Lao, E. A. Lazarus, G. A. Navratil, T. H. Osborne, B. W. Rice, S. A. Sabbagh, J. T. Scoville, E. J. Strait, and T. S. Taylor, *Phys. Rev. Lett.* **82**, 3811 (1999).
- <sup>4</sup>C. M. Bishop, *Plasma Phys. Controlled Fusion* **31**, 1179 (1989).
- <sup>5</sup>R. Fitzpatrick and T. H. Jensen, *Phys. Plasmas* **3**, 2641 (1996).
- <sup>6</sup>M. Okabayashi, N. Pomphrey, and R. E. Hatcher, *Nucl. Fusion* **38**, 1607 (1998).
- <sup>7</sup>R. Fitzpatrick and E. P. Yu, *Phys. Plasmas* **6**, 3536 (1999).
- <sup>8</sup>Y. Q. Liu, A. Bondeson, C. M. Fransson, B. Lennartson, and C. Breitholtz, *Phys. Plasmas* **7**, 3681 (2000).
- <sup>9</sup>C. M. Fransson, B. Lennartson, C. Breitholtz, A. Bondeson, and Y. Q. Liu, *Phys. Plasmas* **7**, 4143 (2000).
- <sup>10</sup>V. D. Pustovitov, *Plasma Phys. Rep.* **27**, 195 (2001).
- <sup>11</sup>Z. R. Wang and S. C. Guo, *Nucl. Fusion* **51**, 053004 (2011).
- <sup>12</sup>M. Okabayashi, J. Bialek, M. S. Chance, M. S. Chu, E. D. Fredrickson, A. M. Garofalo, M. Gryaznevich, R. E. Hatcher, T. H. Jensen, L. C. Johnson, R. J. La Haye, E. A. Lazarus, M. A. Makowski, J. Manickam, G. A. Navratil, J. T. Scoville, E. J. Strait, A. D. Turnbull, and M. L. Walker, *Phys. Plasmas* **8**, 2071 (2001).
- <sup>13</sup>S. A. Sabbagh, R. E. Bell, J. E. Menard, D. A. Gates, A. C. Sontag, J. M. Bialek, B. P. LeBlanc, F. M. Levinton, K. Tritz, and H. Yuh, *Phys. Rev. Lett.* **97**, 045004 (2006).
- <sup>14</sup>S. Ortolani and RFX Team, *Plasma Phys. Controlled Fusion* **48**, B371 (2006).
- <sup>15</sup>E. J. Strait, J. M. Bialek, I. N. Bogatu *et al.*, *Phys. Plasmas* **11**, 2505 (2004).
- <sup>16</sup>P. R. Brunzell, D. Yadikin, D. Gregoratto, R. Paccagnella, T. Bolzonella, M. Cavinato, M. Cecconello, J. R. Drake, A. Luchetta, G. Manduchi, G. Marchiori, L. Marrelli, P. Martin, A. Masiello, F. Milani, S. Ortolani, G. Spizzo, and P. Zanca, *Phys. Rev. Lett.* **93**, 225001 (2004).
- <sup>17</sup>T. Bolzonella, V. Igochine, S. C. Guo, D. Yadikin, M. Baruzzo, and H. Zohm, *Phys. Rev. Lett.* **101**, 165003 (2008).
- <sup>18</sup>R. Betti and J. P. Freidberg, *Phys. Rev. Lett.* **74**, 2949 (1995).
- <sup>19</sup>A. Bondeson and D. J. Ward, *Phys. Rev. Lett.* **72**, 2709 (1994).
- <sup>20</sup>M. S. Chu, J. M. Greene, T. H. Jensen, R. L. Miller, A. Bondeson, R. W. Johnson, and M. E. Mauel, *Phys. Plasmas* **2**, 2236 (1995).
- <sup>21</sup>R. Fitzpatrick and A. Y. Aydemir, *Nucl. Fusion* **36**, 11 (1996).
- <sup>22</sup>H. Reimerdes, A. M. Garofalo, G. L. Jackson, M. Okabayashi, E. J. Strait, M. S. Chu, Y. In, R. J. La Haye, M. J. Lancot, Y. Q. Liu, G. A. Navratil, W. M. Solomon, H. Takahashi, and R. J. Groebner, *Phys. Rev. Lett.* **98**, 055001 (2007).
- <sup>23</sup>E. J. Strait, J. M. Bialek, I. N. Bogatu, M. S. Chance, M. S. Chu, D. H. Edgell, A. M. Garofalo, G. L. Jackson, R. J. Jayakumar, T. H. Jensen, O. Katsuro-Hopkins, J. S. Kim, R. J. La Haye, L. L. Lao, M. A. Makowski, G. A. Navratil, M. Okabayashi, H. Reimerdes, J. T. Scoville, A. D. Turnbull, and DIII-D Team, *Phys. Plasmas* **11**, 2505 (2004).
- <sup>24</sup>M. Takechi, G. Matsunaga, N. Aiba, T. Fujita, T. Ozeki, Y. Koide, Y. Sakamoto, G. Kurita, A. Isayama, Y. Kamada, and JT-60 team, *Phys. Rev. Lett.* **98**, 055002 (2007).
- <sup>25</sup>Bo Hu and R. Betti, *Phys. Rev. Lett.* **93**, 105002 (2004).
- <sup>26</sup>Bo Hu, R. Betti, and J. Manickam, *Phys. Plasmas* **12**, 057301 (2005).
- <sup>27</sup>Y. Q. Liu, M. S. Chu, C. G. Gimblett, and R. J. Hastie, *Phys. Plasmas* **15**, 092505 (2008).
- <sup>28</sup>S. C. Guo, J. P. Freidberg, and R. Nachtrieb, *Phys. Plasmas* **6**, 3868 (1999).
- <sup>29</sup>S. C. Guo, Z. R. Wang, T. Bolzonella, M. Baruzzo, L. Shi, X. G. Wang, "Cylindrical Model of RWM in RFP Plasmas and Application on RFX-mod," in 36th EPS Conference on Plasma Physics, Sofia, June 29–July 3 2009, ECA Vol. 33E, O-5.063.
- <sup>30</sup>D. Yadykin, Y. Q. Liu, and R. Paccagnella, *Plasma Phys. Controlled Fusion* **53**, 085024 (2011).
- <sup>31</sup>J. S. Sarff, J. K. Anderson, T. M. Biewer, D. L. Brower, B. E. Chapman, P. K. Chattopadhyay, D. Craig, B. Deng, D. J. Den Hartog, W. X. Ding, G. Fiksel, C. B. Forest, J. A. Goetz, R. O'Connell, S. C. Prager, and M. A. Thomas, *Plasma Phys. Controlled Fusion* **45**, A457 (2003).
- <sup>32</sup>Y. Q. Liu, M. S. Chu, I. T. Chapman, and T. C. Hender, *Phys. Plasmas* **15**, 112503 (2008).
- <sup>33</sup>T. M. Antonsen and Y. C. Lee, *Phys. Fluids* **25**, 132 (1982).
- <sup>34</sup>F. Porcelli, R. Stankiewicz, W. Kerner, and H. L. Berk, *Phys. Plasmas* **1**, 470 (1994).

- <sup>35</sup>I. B. Bernstein, E. A. Frieman, M. D. Kruskal, and R. M. Kulsrud, *Proc. R. Soc. London* **244**(1236), 17–40 (1958).
- <sup>36</sup>J. P. Freidberg, *Ideal Magnetohydrodynamics* (Plenum, New York, 1987); *Plasma Physics and Fusion Energy* (Cambridge University Press, 2007).
- <sup>37</sup>M. S. Chu and M. Okabayashi, *Plasma Phys. Controlled Fusion* **52**, 123001 (2010).
- <sup>38</sup>Z. R. Wang, S. C. Guo, L. Shi, T. Bolzonella, M. Baruzzo, and X. G. Wang, *Phys. Plasmas* **17**, 052501 (2010).
- <sup>39</sup>S. Ortolani and D. D. Schnack, *Magnetohydrodynamics of Plasma Relaxation* (World Scientific, 1993).
- <sup>40</sup>P. Sonato, G. Chitarin, P. Zaccaria, F. Gnesotto, S. Ortolani, A. Buffa, M. Bagatin, W. R. Baker, S. Dal Bello, P. Fiorentin, L. Grando, G. Marchiori, D. Marcuzzi, A. Masiello, S. Peruzzo, N. Pomaro, and G. Serianni, *Fusion Eng. Des.* **66–68**, 161 (2003).
- <sup>41</sup>S. W. Haney and J. P. Freidberg, *Phys. Fluids B* **1**, 1637 (1989).
- <sup>42</sup>J. W. Berkery, S. A. Sabbagh, R. Betti, B. Hu, R. E. Bell, S. P. Gerhardt, J. Manickam, and K. Tritz, *Phys. Rev. Lett.* **104**, 035003 (2010).
- <sup>43</sup>J. W. Berkery, S. A. Sabbagh, R. Betti, R. E. Bell, S. P. Gerhardt, B. P. LeBlanc, and H. Yuh, *Phys. Rev. Lett.* **106**, 075004 (2011).
- <sup>44</sup>Z. R. Wang, S. C. Guo, Y. Q. Liu, and M. S. Chu, *Nucl. Fusion* **52**, 063001 (2012).
- <sup>45</sup>R. Paccagnella, D. D. Schnack, and M. S. Chu, *Phys. Plasmas* **9**, 234 (2002).
- <sup>46</sup>R. Paccagnella, S. Ortolani, P. Zanca, A. Alfier, T. Bolzonella, L. Marrelli, M. E. Puiatti, G. Serianni, D. Terranova, M. Valisa, M. Agostini, L. Apolloni, F. Auriemma, F. Bonomo, A. Canton, L. Carraro, R. Cavazzana, M. Cavinato, P. Franz, E. Gazza, L. Grando, P. Innocente, R. Lorenzini, A. Luchetta, G. Manduchi, G. Marchiori, S. Martini, R. Pasqualotto, P. Piovesan, N. Pomaro, P. Scarin, G. Spizzo, M. Spolaore, C. Taliercio, N. Vianello, B. Zaniol, L. Zanotto, and M. Zuin, *Phys. Rev. Lett.* **97**, 075001 (2006).
- <sup>47</sup>Y. Q. Liu, M. S. Chu, I. T. Chapman, and T. C. Hender, *Nucl. Fusion* **49**, 035004 (2009).